International Journal of Rock Mechanics & Mining Sciences 129 (2020) 104285

Contents lists available at ScienceDirect

International Journal of Rock Mechanics and Mining Sciences

journal homepage: http://www.elsevier.com/locate/ijrmms

Influence of cooling rate on thermal degradation of physical and mechanical properties of granite

Fan Zhang [a], Yuhao Zhang [a], Yudong Yu [a], Dawei Hu [b], Jianfu Shao [a,c,*]

[a] School of Civil Engineering, Architecture and Environment, Hubei University of Technology, Wuhan, 430068, China
[b] State Key Laboratory of Geomechanics and Geotechnical Engineering, Institute of Rock and Soil Mechanics, Chinese Academy of Sciences, Wuhan, 430071, China
[c] University of Lille, CNRS, FRE2016, LaMcube, 59000, Lille, France

ARTICLE INFO

Keywords:
Granite
Physical and mechanical properties
Thermal effect
Heating and cooling
Thermal cracking
Compression strength

ABSTRACT

Large temperature changes may cause degradation in physical and mechanical properties of rocks. This degradation can be influenced by heating-cooling procedure. In this study, it is proposed to investigate the influence of cooling method after heating to high temperature on the degradation of physical and mechanical properties of granite. For this purpose, two different cooling procedures are considered, the rapid cold water cooling and the slow step-by-step cooling. Two groups of granite samples are first heated to a desired temperature ranging from 25 °C to 900 °C, and then cooled respectively by using these two methods. The porosity and ultrasonic velocity of the thermally treated samples are measured. Uniaxial and triaxial compression tests are also performed to evaluate the elastic properties and compression strength. It is found that for both groups of samples, the thermal treatment induces the porosity increase, the wave velocity decrease and the modification of elastic modulus and compression strength. But the modification of mechanical properties is clearly influenced by the thermal treatment procedure.

1. Introduction

Hot dry rock (HDR) resources, recognized as an efficient, low-carbon, clean energy source, has attracted more and more attention in recent years with the depletion of fossil energy sources and the increasingly severe environmental problems. The amount of hot dry rock resources stored in the world is dozen times of the total storage capacity of oil and natural gas.[1,2] HDR energy is widely distributed in granite at depth of 2–6 km where the temperature is about 150–650 °C.[3] Nitrogen, sulfur oxides and other pollutants are barely produced during development and utilization of HDR, and no other pollution problems will arise.[3,4] The usual mining method of HDR resources is to drill wells into hot rock formations, and then to inject cold water into the wells so that cold water can be absorbed by the rock masses and fissures, where the heat energy is converted into hot fluid, and the energy is finally converted by using the discharged water vapor or hot water to liquefy into liquid water to release thermal energy. Therefore, it is of great scientific value and practical significance to deeply study the mechanism and deformation characteristics of rock cracking mechanisms after high temperature heat treatment and cooling for the design and exploitation of deep hot rock geothermal resources.

A large number of experimental studies have been performed to investigate the mechanical properties of rocks after high temperature heating and natural cooling treatment.[5–15] Most previous studies have shown that the mechanical and physical properties of rock materials are weakened at high temperature (peak strength and elastic modulus decrease, permeability and porosity increase). The variations in porosity, P-wave velocity, elastic modulus, and peak strength are all related to the heat treatment temperature.[16–27] Vagnon et al.[28] investigated the mechanical properties of marble at high temperature and shown that the thermal cracking yielded porosity increase and weakening of physical and mechanical properties of rocks. Some other experimental studies have been also performed on the mechanical properties of rock subjected to high temperature heating and rapid cooling treatment.[29–33] The heating and rapid cooling treatment lead to a complex stress distribution in crystalline rocks due to mineral thermal expansion and the non-uniform temperature distribution,[34–36] and the mechanical strength, elastic modulus and fracture toughness decrease, while the permeability and porosity increase, and the material anisotropy is attenuated.[37,38] It seems that there is a difference in the effect on properties of rock materials between rapid cooling and natural cooling because of temperature gradients and thermal shock.[39–43] However,

* Corresponding author. School of Civil Engineering, Architecture and Environment, Hubei University of Technology, Wuhan, 430068, China.
E-mail address: jian-fu.shao@polytech-lille.fr (J. Shao).

https://doi.org/10.1016/j.ijrmms.2020.104285
Received 17 May 2019; Received in revised form 26 February 2020; Accepted 26 February 2020
Available online 12 March 2020
1365-1609/

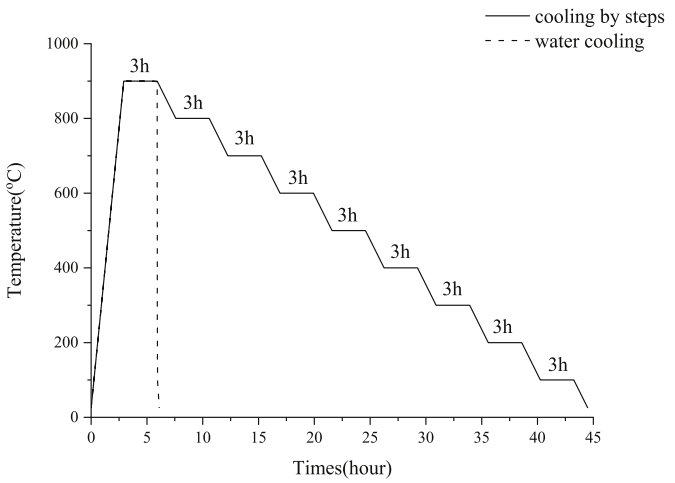

Fig. 1. Schematic illustration of heating and cooling procedures.

there are few experimental studies on the effect of cooling rate on thermal degradation of mechanical properties.

In this paper, we shall compare two different cooling methods, the rapid water cooling and the slow step-by-step cooling. Two groups of granite samples will be heated to a desired temperature and then cooled by these two methods. The porosity and sonic velocity of both groups of samples will be measured. Uniaxial and triaxial compression tests will also be performed. By comparing the results obtained from two groups of samples, we will characterize the effect of cooling method on the thermal degradation of physical and mechanical properties of granite.

2. Samples preparation and thermal treatment

2.1. Rock description and samples preparation

The samples are drilled from fresh fine and uniform grained granite blocks, selected in Dabie Mountain, Macheng, Hubei province, China. The main mineral composition of the granite based on the X-ray diffraction analysis is quartz (8.9%), potassium feldspar (45.1%), albite (21.1%), mica (23.2%), green mud stone (1.7%) and calcite (0.2%). The natural density of granite is about 2.60 g/cm^3. The diameter and height of cylindrical samples is respectively about 37 ± 0.02 mm and 74 ± 0.05 mm.

2.2. Thermal treatment

As the main purpose of this work is to investigate the influence of thermal treatment procedure on mechanical properties of granite, two different procedures are chosen. In the first procedure, the samples are first heated at a rate of 5 °C/min until a desired temperature and then cooled in cold water. In the second procedure, the samples are first heated with the same rate as that in the first procedure, but then step-by-step cooled. The heating rate used here (5 °C/min) is considered as low enough in order to reduce the effect of thermal gradient inside the samples so that the thermal effect can be entirely attributed to temperature raise.[40,43–48] Four levels of heating temperature are selected, namely 200 °C, 400 °C, 600 °C and 900 °C. A schematic illustration of heating and cooling steps is shown in Fig. 1 for both the water cooling and step-by-step cooling methods. For the heating and water cooling procedure, after a stabilization period of 3 h at the desired heating temperature, the samples are suddenly immersed into room-temperature water in a container with a volume of 25 L. For the heating and step-by-step cooling procedure, the samples are first cooled in a furnace to ambient pressure at a rate of 1 °C/min until the selected temperature is reached. After a stabilization period of 3 h, the temperature is decreased to the next cooling step. The temperature decrease for

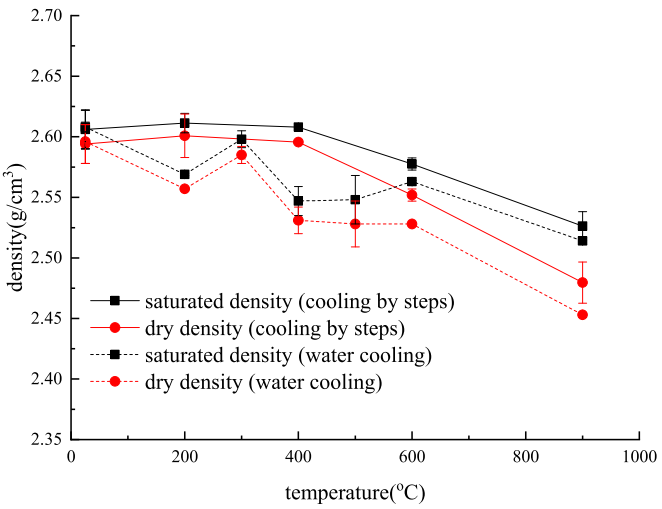

(a) Evolution of density

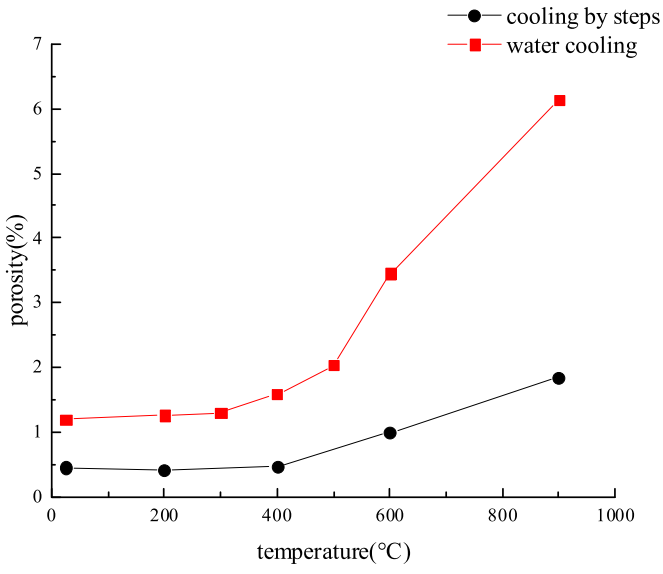

(b) Evolution of porosity

Fig. 2. Evolution of density (a) and porosity (b) with heat treatment temperature for two different cooling methods.

each cooling step is 100 °C. Again, this low cooling rate is adopted to reduce the temperature gradient in the samples. Finally, all the samples are conserved in a desiccator until the completion of subsequent tests.

3. Physical and mechanical properties

3.1. Porosity

Porosity is one of the fundamental physical properties of porous rocks. In this study, the porosity of the measurement test is measured by the conventional wetting-drying method. The samples are saturated by water in vacuum. The saturation is considered as completed when the weight variation of samples within one week is less than 0.1% of the total mass. The mass and volume of each sample is measured. The samples are then dried in an oven at 105 °C for 24 h. Each sample is considered as fully dried when the variation of its mass is less than 0.1%

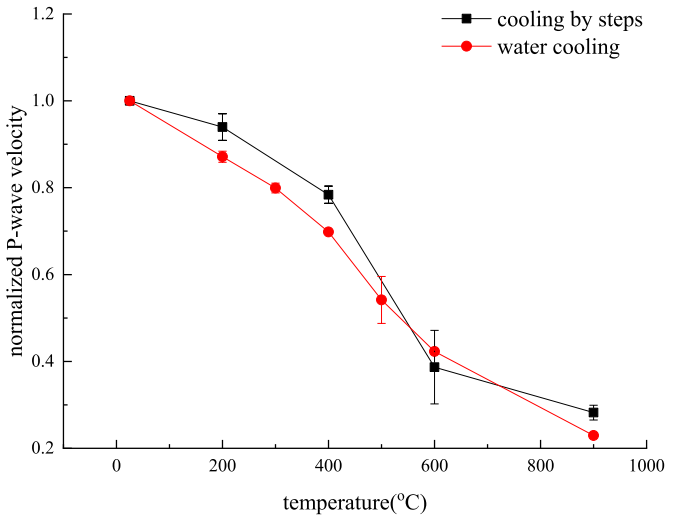

Fig. 3. Evolutions of P-wave velocity of samples treated with two different cooling methods.

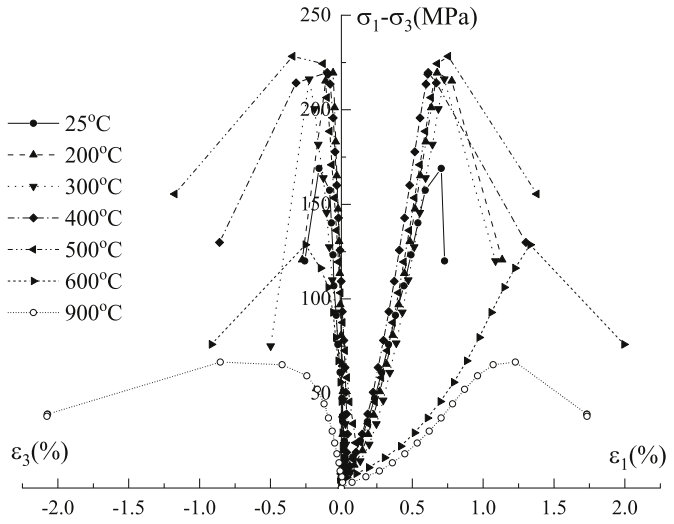

Fig. 5. Typical stress-strain curves in uniaxial compression tests of granite samples treated by water cooling method.

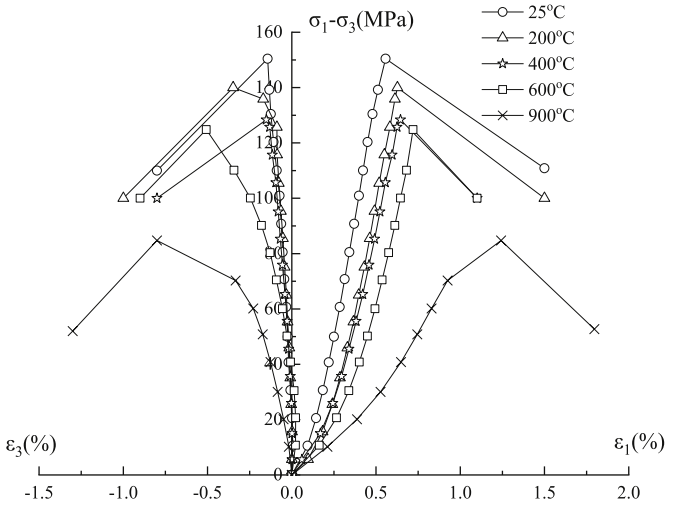

Fig. 4. Typical stress-strain curves in uniaxial compression tests of granite samples treated by step-by-step cooling method.

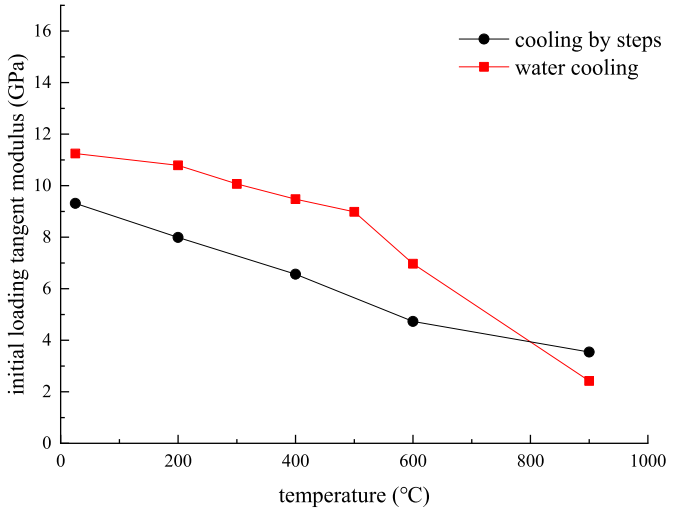

Fig. 6. Variation of initial loading tangent modulus in uniaxial compression tests with heating temperature for two different cooling methods.

of the total mass during drying process. The mass and volume of each dry sample are measured. The porosity and density are then calculated from the mass and volume of the saturated and dry states of each sample. The values of density and porosity of the samples for different heating temperatures are given in Table 1 of Appendix and presented in Fig. 2, for the sake of comparison; the following normalized porosity is here used:

$$n = \frac{n_t}{n_{25°C}} \quad (1)$$

In Fig. 2(a), one can see that both the saturated and dry densities decrease with the heat treatment temperature for the two cooling procedures. However, the density decrease of the water-cooled samples has some fluctuations while that of the step cooled samples is regular. When the temperature is higher than 573 °C, the decrease of dry density with heat treatment temperature is generally considered as a consequence of quartz transformation from α-type to β-type.[49,50] This transformation can produce a volume expansion of about 0.45%.[51] According to the results in Fig. 2(b), the porosity change is very small when the heating temperature is below 400 °C. That implies that the samples exhibit only some minor structural changes below 400 °C, primarily due to the opening of pre-existing microcracks and/or to the nucleation of some new microcracks during the heating and cooling phases.[19] The porosity change is clearly accelerated when the heating temperature is higher than 400 °C. The porosity change of the water-cooled samples seems to be more significant than that of the step-by-step cooled samples. This difference seems to indicate that the rapid water cooling method generates more important thermal degradation of granite microstructure than the slow step-by-step cooling method, such as the α-β type transition in crystal structure enhancing the connection of microcrack networks and an increase in the number of open micro-cracks.[52]

3.2. Ultrasonic velocity

The evolution of normalized P-wave velocity with thermal treatment temperature is presented in Fig. 3, for two different thermal treatment methods. It is found that the ultrasonic velocity decreases with the increase of heating temperature and there is no significant difference between the two cooling methods. The rate of the P-wave velocity decrease slows down after 400 °C. This decrease of ultrasonic velocity is also generally attributed to the generation of microcracks during heating and cooling processes.

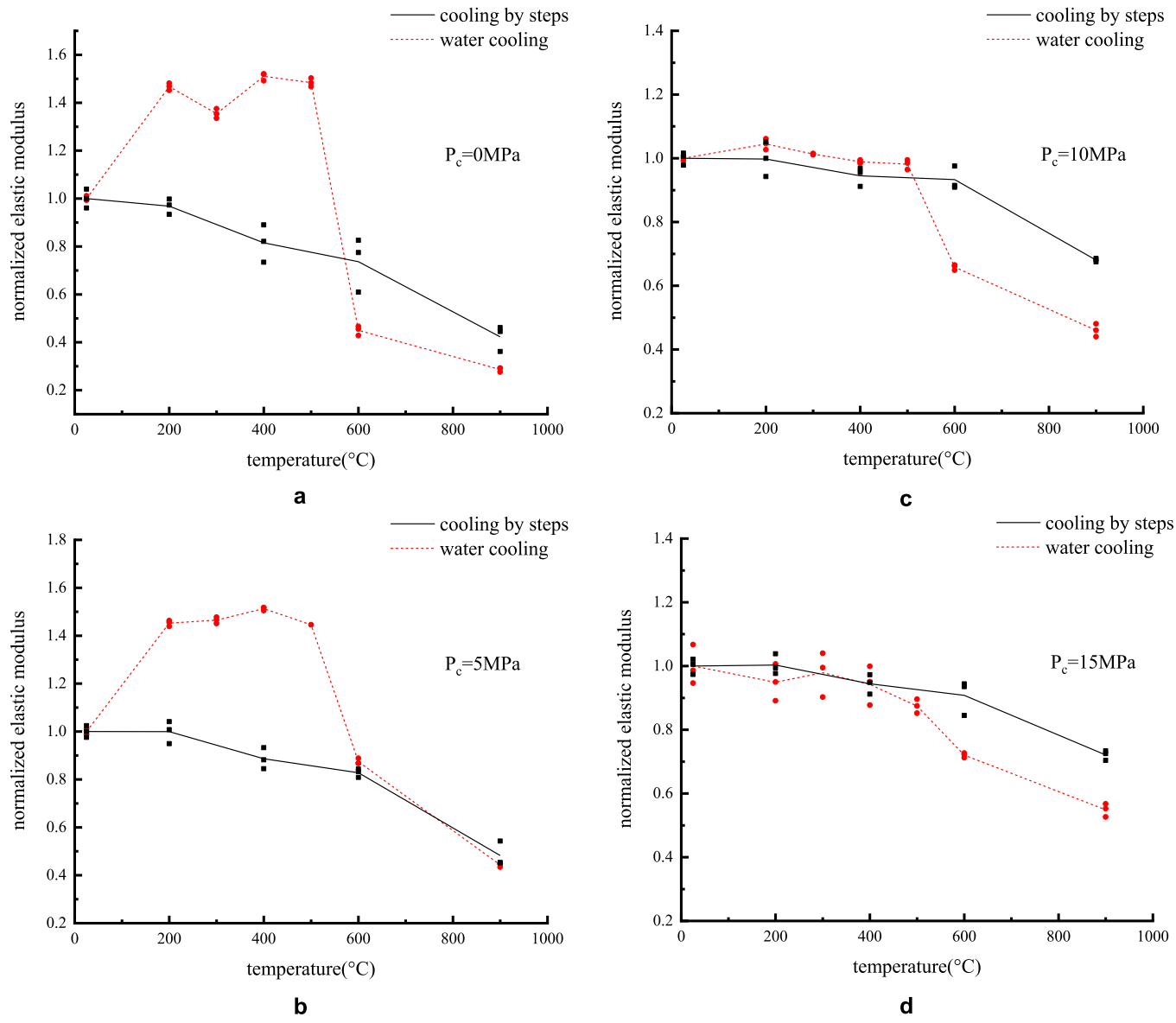

Fig. 7. Evolution of elastic modulus of samples after two different thermal treatments.

3.3. Mechanical responses

Uniaxial and triaxial compression tests are performed on two groups of granite samples. The typical stress-strain curves in uniaxial compression tests of the samples treated by the step-by-step cooling method are presented in Fig. 4. We can see that the mechanical responses are significantly influenced by the thermal treatment temperature. For all values of temperature, there is a nonlinear concave phase at the beginning of axial (deviatoric) stress loading. This phase is generally related to the progressive closure of existing microcracks generated during the preparation and thermal treatment of samples.[53] It is interesting to see that this initial nonlinear phase is much more pronounced when the heating temperature is higher. This confirms that the thermal treatment induces the generation and development of microcracks.[54–56] After the closure of microcracks, a quasi linear stress-strain phase is observed and this phase represents the elastic deformation of the material. It is found that the linear elastic phase is longer and easier to identify when the thermal treatment temperature is lower. After the linear elastic phase, one can observe a more or less marked nonlinear phase before the peak stress is reached. This nonlinear phase can be related to the nucleation and growth of new microcracks.[57] It is interesting to observe that this pre-peak nonlinear phase is more marked when the heating temperature is higher. From the results given in these tests, it is clear that the uniaxial compression strength (UCS) is significantly deteriorated by the thermal treatment and this degradation is much greater when the temperature is higher. Further, it seems that the high heating temperature enhances less stiff behavior of granite. In Fig. 5, we show the stress-strain curves in uniaxial compression tests of samples treated by the rapid water cooling method. Similar remarks as those for the samples treated by the step-by-step cooling method can be made. More discussions on the effect of cooling method are presented in the next section.

4. Analyses

In order to better characterize the effect of cooling method, some quantitative comparisons are presented in this section. The initial tangent modulus is first calculated at very beginning of loading stress-strain curve in uniaxial compression tests. The obtained values are given in Table A1 of Appendix and plotted in Fig. 6. The initial tangent modulus of thermally treated samples continuously decreases with the heating temperature for the two cooling methods. However, for the

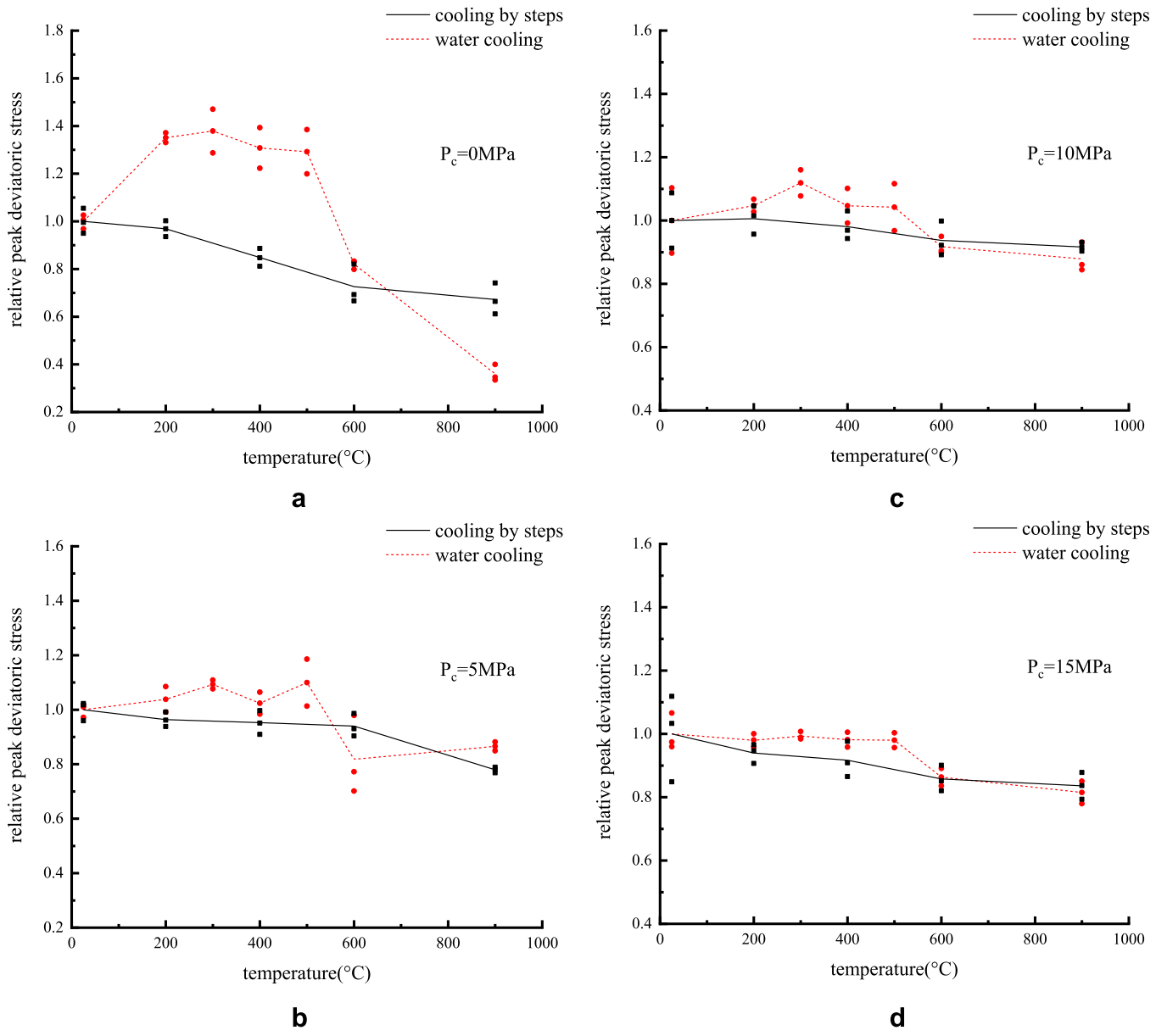

Fig. 8. Variation of relative peak deviatoric stress of samples after two different thermal treatments.

samples cooled by the step-by-step method, the rate of initial tangent modulus is reduced after the temperature reaches 600 °C. On the contrary, in the sampled rapidly cooled by cold water, the decrease of initial modulus is accelerated when the temperature is higher than 500 °C.

As mentioned above, in each stress-strain curve, it is possible to identify a quasi linear part after the closure of initial microcracks and before the nucleation and propagation of new microcracks. This linear part is here interpreted as the elastic phase of material. We have calculated the elastic modulus and Poisson's ratio from this linear part in uniaxial and triaxial compression tests. The obtained values are given in Table A3 and Table A4 of Appendix. In Fig. 7, we show the evolution of normalized elastic modulus of samples treated by two different cooling methods. We can see that when the heating temperature is between 25 °C and 500 °C, the elastic modulus of cold water-cooled samples increases with the heating temperature under low confining pressures (0 and 5 MPa) while the elastic modulus of step-by-step cooled samples continuously decreases. This kind of difference is generally related to two physical processes under competition: the thermal hardening and cracking.[5,6] Indeed, when granite samples are heated and rapidly cooled by cold water, the related strong temperature gradient can generate an important local stress concentration which induces a non-uniform plastic strain field in the samples. For the samples that are step-by-step cooled, the rate of cooling is slow and this reduces the local stress concentration and the non-uniform plastic strain field. As a consequence, for the range of temperature and confining pressure considered, the plastic hardening is dominating on the thermal cracking in the cold water cooled samples while the opposite process occurs in the step-by-step cooled samples. When the heating temperature is higher than 600 °C, there is an acceleration of elastic modulus decrease for both groups of samples. On the other hand, it is found that it is not easy to give a clear trend for the variation of Poisson's ratio and there is no significant difference between two cooling methods.

The experimental values of peak deviatoric stress are also determined and given in Table A5 of Appendix. The evolutions of normalized peak stress of samples treated by two cooling methods are plotted in Fig. 8. We can clearly see that the uniaxial compression strength of the samples treated by the water cooling method exhibits a significant increase from 25 °C to 500 °C. But there is no such strength increase in the

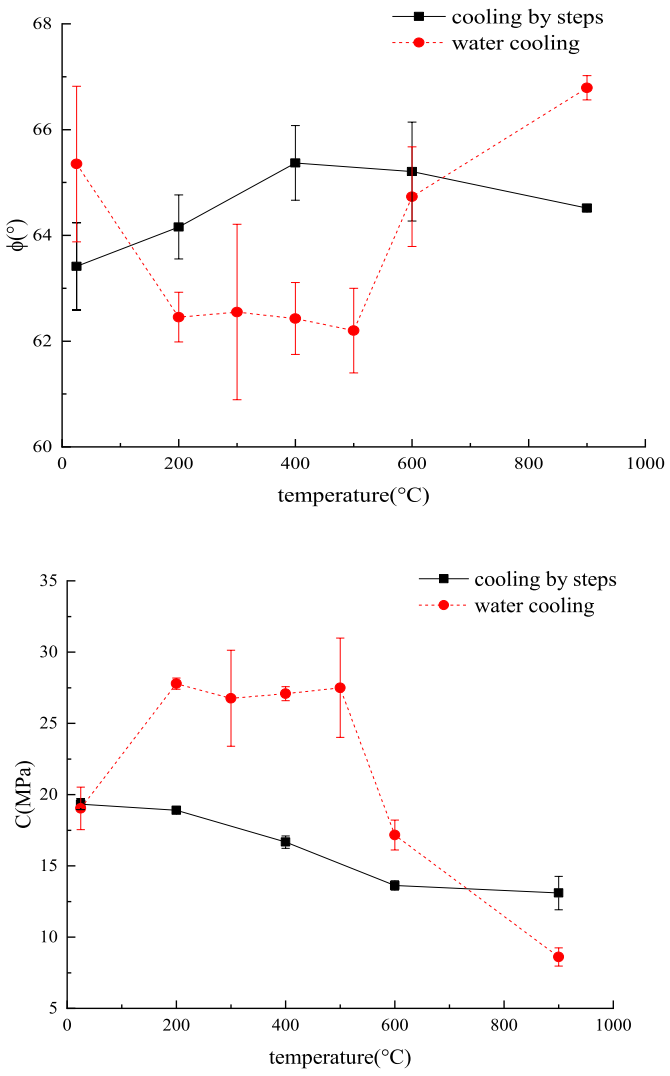

Fig. 9. Variation of cohesion and friction angle of samples after two different thermal treatments.

samples treated by the step cooling method. However, with the increase of confining pressure, the difference of peak strength evolution becomes small between the samples treated by the two different cooling methods. It seems that the evolution of peak stress is in agreement with that of elastic modulus.

From the experimental values of peak stress obtained from the uniaxial and triaxial compression tests, it is possible to calculate the two common strength parameters by using the following classical Mohr-Coulomb failure criterion:

$$F = \frac{1}{2}(\sigma_1 - \sigma_3) + \frac{1}{2}(\sigma_1 + \sigma_3)\sin\phi - c\cos\phi = 0 \quad (2)$$

σ_1 and σ_3 are respectively the major and minor principal stress. c and ϕ denote the cohesion coefficient and the frictional angle. The obtained values of c and ϕ are given in Table A6 of Appendix for the groups of samples. The evolutions of c and ϕ are plotted in Fig. 9. The friction angle of the step-by-step cooled samples increases with the temperature up to 600 °C, and then slightly decreases between 600 °C and 900 °C. However, the friction angle of the cold water-cooled samples decreases with the heating temperature until 500 °C, and then increases between 500 °C and 900 °C. The cohesion of the step-by-step cooled samples continuously decreases with the heat treatment temperature. But the cohesion of the cold water-cooled samples first increases between 25 °C and 500 °C and then considerably decreases when the temperature exceeds 500 °C. It seems that in the rapid cooled samples, for range of 25 °C and 500 °C, the rapid cooling rate induces high local thermal stresses and strong cooling-related shrinkage of samples. This has a preventing effect on the development of thermal cracks and results in an increase of material cohesion. When the temperature is greater than 500 °C, a large number of thermal cracks are created so that the material cohesion is significantly reduced. However, in the step-by-step cooled samples, the effect of thermal shrinkage due to thermal stresses is less important. Therefore, the material cohesion continuously decreases due to thermal cracking.

5. Discussions

There is a competition between the thermal cracking and hardening.[5,6,57] It is said that thermal cracks develop mostly during heating.[58,59] However, high temperature gradients due to rapid water cooling will cause thermal hardening which induces high local thermal stresses and strong cooling-related shrinkage of samples. This has a preventing effect on the development of thermal cracks. Therefore, the generation and development of thermal cracks are influenced by the combined effects of thermal cracking and hardening. According to the experimental data presented above, it can be seen that the thermal cracking caused by thermal treatment will induce the physical and mechanical properties of granite to decline to different degrees. When the thermal cracking is dominating, the physical and mechanical properties of the samples decrease. On the contrary, when the thermal hardening plays an essential role, there is an obvious “hardening effect” which can be seen clearly in some parameters.

For the mechanical parameters such as elastic modulus, compression strength, internal friction angle and cohesion, it can be seen that the water-cooled samples have a significant hardening effect up to 500 °C. This is not the case for the step-by-step cooled samples. For the physical parameters such as porosity and ultrasonic velocity, the hardening effects are not clearly demonstrated. For the water-cooled samples, the evolution of wave velocity, porosity and initial loading tangent modulus is monotonic with temperature. When the high temperature heated granite is rapidly put into water, the outer surface of sample is rapidly cooled, inducing a non-uniformed plastic strain field. And the strength of the outer surface is rapidly increased while the mineral particles inside sample are not cooled synchronously with its outer surface during the rapid cooling process. Therefore, the deformation caused by thermal expansion is restrained by the outer surface of sample and its inner compactness increases. However, as the degree of compactness increases, a certain amount of thermal cracks are also generated. It makes some parameters (e.g. porosity, ultrasonic velocity, initial loading tangent modulus) evolve monotonically without showing an obvious “hardening effect” as for the peak strength and elastic modulus. In addition, it is seen in Figs. 7 and 8 that the hardening effect is attenuated as the confining pressure increases. The effect of confining pressure limits the volume change and increases the ductility of samples. Therefore, the compression strength of sample is increased and the stiffness of sample is also restricted.

In HDR project, the premise of efficient heat extraction is to generate a good artificial fracture network in reservoir.[3,60,61] In addition to hydraulic fracturing, the high temperature thermal reservoir rock mass during hydraulic fracturing also has a large temperature gradient, and it will cause thermal degradation.[31,60,62] In order to better investigate HDR thermal reservoirs, the depth is also one of the important factors.[63] The confining pressure is increasing with the depth. According to the present results, the thermal hardening effect is attenuated at high confining pressure. And the increase in temperature caused by a small increase in depth has no significant effect on rock properties compared to the confining pressure.[64] Thus, we can imagine that the thermal hardening effect is also reduced as the depth increases. Moreover, the distribution, angle and development of cracks induce the degradation of mechanical behavior.[65] The distribution and development of thermal

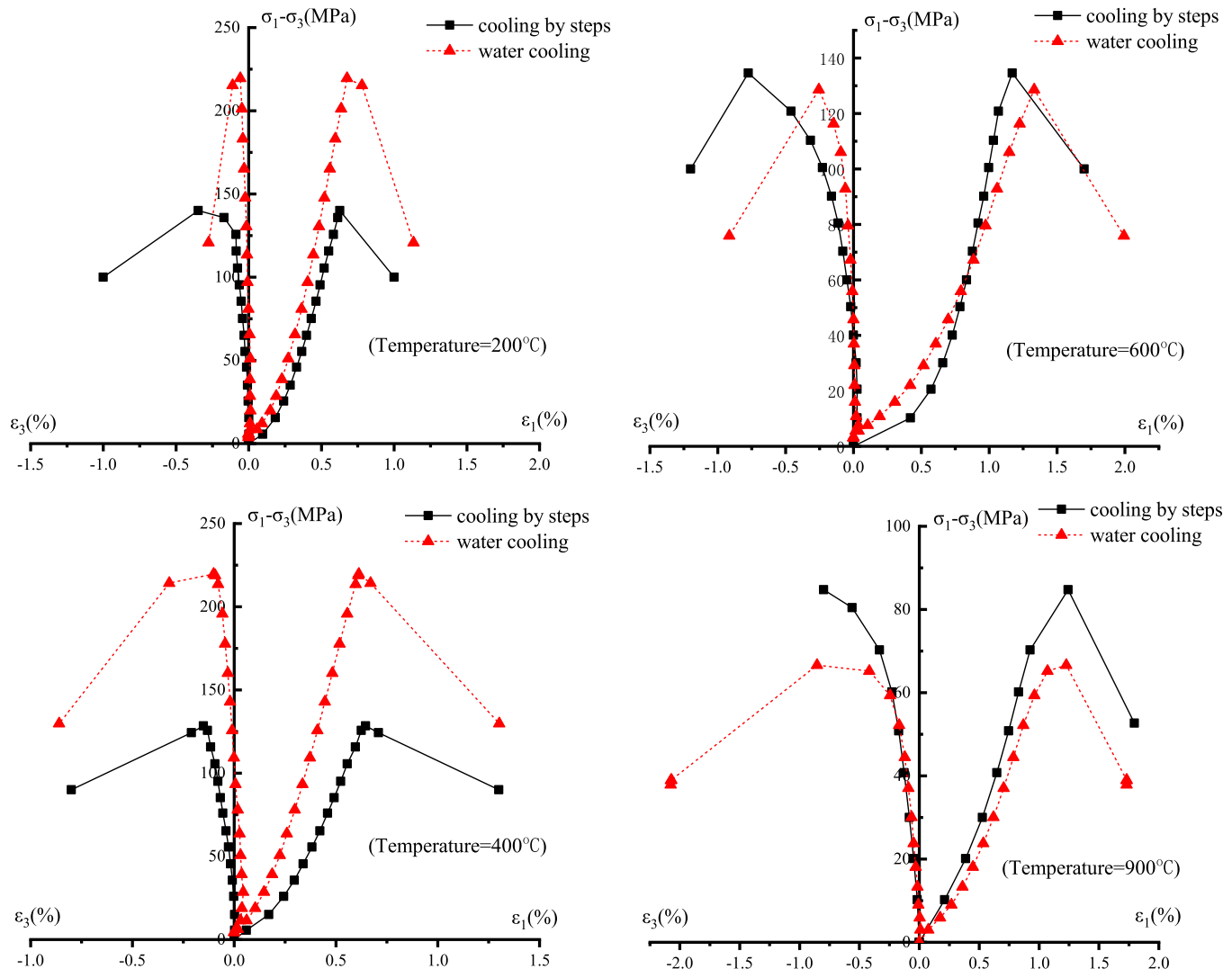

Fig. A1. Comparison of stress-strain curves in uniaxial compression tests between two different cooling methods.

cracks generated in heating-cooling process are related to factors such as temperature and confining pressure. It can be quantitatively characterized in our future study. In addition, it is interesting to notice that the results of the present study show that the thermal hardening enhances the mechanical properties of granite in a certain temperature range, and the transport properties are also enhanced. It has very positive significance for the HDR thermal reservoir engineering.

6. Conclusions

In this paper, we have investigated the degradation of physical and mechanical properties of granite samples subjected to two different heating-cooling methods, in particular the evolution of porosity, wave velocity, elastic modulus and compression strength. It is found that the high cooling rate induces important thermal stresses. It is manifested by the fact that the thermal hardening is the dominant process in the samples treated by the cold water cooling. This induces an increase in elastic modulus and peak strength when the heating temperature is lower than 500 °C. This phenomenon is not observed in the samples treated by the step-by-step cooling. When the heating temperature is higher than 500 °C, there is a significant decrease in elastic modulus and peak strength for two groups of samples. This is due to the effect of thermally induced micro-cracks with a clear increase in porosity. The thermal degradation of compression strength of granite sample is also influenced by the cooling method. In relation with the elastic modulus, in the samples cooled by the cold water method, the cohesion first increases until 500 °C and then decreases when the heating temperature is higher. However, for the samples cooled by the step method, the cohesion is continuously decreasing with the heating temperature. The friction angle of samples exhibits an opposite trend. As a conclusion, the rapid cooling treatment can result in a reinforcement of elastic modulus and compression strength until 500 °C and then a sharp decrease of those properties when the heating temperature is higher. On the other hand, the slow cooling treatment generates a progressive degradation of elastic modulus and compression strength of granite.

Declaration of competing interest

We declare that there is no conflict of interest.

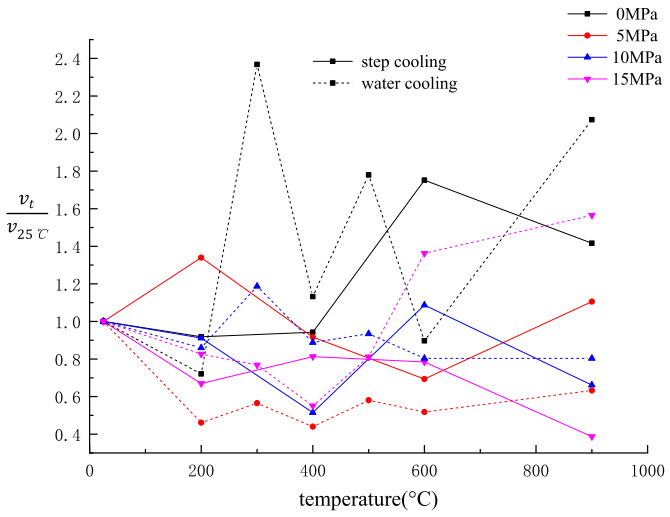

Fig. A2. Variation of normalized Poisson's ratio between two different cooling methods.

Acknowledgements

The financial support by the National Key Research and Development Program of China (Grant Nos. 2018YFC0809600 and 2018YFC0809601), National Natural Science Foundation of China (Grant Nos. 51979100 and 51779252), and Major Technological Innovation Projects of Hubei, China (Grant No. 2017AAA128) for this work are gratefully acknowledged.

Appendix

Table A1
Density and porosity of granite samples after two different thermal treatments

Temperature (°C)		25	200	400	600	900
ρ_{sat} (g/cm^3)	water cooling	2.6082	2.5698	2.5477	2.5632	2.5146
	step cooling	2.6053	2.6107	2.6079	2.5773	2.5263
ρ_d(g/cm^3)	water cooling	2.5962	2.5572	2.5319	2.5287	2.4533
	step cooling	2.5937	2.6003	2.5950	2.5513	2.4793
Porosity (%)	water cooling	1.1916	1.2583	1.5802	3.4493	6.1308
	step cooling	0.4537	0.4033	0.4733	0.9933	1.8433

Table A2
Initial loading tangent modulus measured in uniaxial compression tests

Temperature (°C)		25 °C	200 °C	400 °C	600 °C	900 °C
E_0(GPa)	Water cooling	11.2467	10.7908	9.4745	6.9709	2.4198
	Step cooling	9.315	7.9933	6.5633	4.7333	3.54

Table A3
Elastic modulus of samples after two different thermal treatments

Confining pressure (MPa)		Elastic modulus						
		25 °C	200 °C	300 °C	400 °C	500 °C	600 °C	900 °C
0	Water cooling	30.74	45.76	41.24	46.08	45.32	14.06	9.03
		30.68	44.85	41.80	46.93	45.80	13.22	9.01
		31.24	45.35	42.47	46.94	46.41	14.40	8.53
	Step cooling	33.02	30.84	/	24.25	/	20.12	11.95
		34.32	32.95		27.12		25.57	14.69
		31.72	32.12		29.39		27.27	15.23
5	Water cooling	32.79	47.74	48.15	49.93	47.96	28.79	14.85
		33.18	48.53	49.02	50.33	47.96	28.78	14.87
		33.58	48.29	48.66	50.34	47.96	29.47	14.40
	Step cooling	43.17	40.98	/	40.25	/	34.90	19.5
		44.23	43.51		36.47		35.95	19.55
		42.11	44.94		38.06		36.40	23.43
10	Water cooling	52.17	53.97	53.33	51.70	50.68	34.10	24.18
		52.55	55.77	53.31	52.27	52.27	34.75	25.25
		52.95	54.99	53.13	51.97	51.78	34.94	23.12
	Step cooling	44.58	42.95	/	43.52	/	44.46	30.74
		46.30	45.56		41.55		41.42	31.05
		45.83	47.89		44.11		41.68	31.26

(*continued on next page*)

Table A3 (*continued*)

Confining pressure (MPa)		Elastic modulus						
		25 °C	200 °C	300 °C	400 °C	500 °C	600 °C	900 °C
15	Water cooling	58.67	55.33	57.18	48.24	48.09	39.17	28.93
		54.23	52.21	54.70	52.26	46.84	39.70	31.19
		52.02	48.98	49.62	54.92	49.25	39.95	30.38
	Step cooling	46.45	45.13	/	44.97	/	39.05	32.53
		47.21	45.95		42.14		43.23	33.51
		45.00	48.00		43.84		43.63	33.91

Table A4
Poisson's ratio of samples after two different thermal treatments

Confining pressure (MPa)		Poisson's ratio						
		25 °C	200 °C	300 °C	400 °C	500 °C	600 °C	900 °C
0	Water cooling	0.23	0.17	0.56	0.19	0.41	0.24	0.39
		0.23	0.16	0.53	0.28	0.39	0.17	0.50
		0.22	0.16	0.52	0.30	0.41	0.20	0.52
	Step cooling	0.33	0.30		0.31		0.58	0.47
		0.37	0.29		0.30		0.56	0.48
		0.30	0.32		0.33		0.63	0.45
5	Water cooling	0.68	0.30	0.39	0.28	0.34	0.39	0.41
		0.64	0.29	0.35	0.27	0.38	0.28	0.38
		0.61	0.30	0.35	0.30	0.40	0.33	0.43
	Step cooling	0.24	0.33		0.22		0.17	0.27
		0.26	0.32		0.21		0.16	0.25
		0.25	0.34		0.24		0.18	0.28
10	Water cooling	0.36	0.33	0.41	0.32	0.35	0.31	0.20
		0.34	0.28	0.42	0.30	0.31	0.29	0.27
		0.37	0.31	0.44	0.33	0.34	0.26	0.39
	Step cooling	0.44	0.40	/	0.23	/	0.48	0.29
		0.46	0.39		0.21		0.42	0.28
		0.45	0.42		0.26		0.51	0.30
15	Water cooling	0.28	0.20	0.21	0.11	0.13	0.34	0.31
		0.25	0.11	0.11	0.12	0.18	0.30	0.45
		0.16	0.26	0.21	0.15	0.25	0.30	0.32
	Step cooling	0.60	0.40	/	0.49	/	0.47	0.23
		0.60	0.35		0.47		0.45	0.20
		0.61	0.47		0.51		0.48	0.27

Table A5
Peak deviatoric stress of samples after two different thermal treatments

Confining pressure (MPa)		Peak deviatoric stress (MPa)						
		25 °C	200 °C	300 °C	400 °C	500 °C	600 °C	900 °C
0	Water cooling	168.98	223.52	247.05	205.44	201.45	134.15	67.12
		172.33	230.33	216.22	233.98	232.65	139.95	58.18
		162.67	226.93	231.63	219.71	217.05	139.56	56.18
	Step cooling	143.86	141.71	/	128.33	/	124.19	92.61
		150.74	151.76		122.94		100.89	100.56
		159.71	146.73		134.23		104.86	112.32
5	Water cooling	299.70	319.44	326.45	313.33	298.35	227.45	259.63
		297.37	291.94	316.98	289.67	349.04	206.57	250.05
		286.09	305.69	321.71	301.50	323.69	288.26	254.84
	Step cooling	316.20	297.25	/	308.12	/	304.92	241.3
		314.57	290.02		294.01		287.52	237.56
		296.56	306.52		281.16		279.37	243.93
10	Water cooling	406.68	393.60	397.31	365.76	411.59	331.29	343.42
		330.87	378.88	427.80	406.06	356.89	350.19	311.46
		368.77	386.24	412.56	385.91	384.24	333.61	317.36
	Step cooling	416.00	366.12	/	394.22	/	381.97	345.62
		349.33	400.23		360.85		352.60	350.29
		382.66	388.34		370.89		341.23	356.33
15	Water cooling	441.40	460.06	454.69	440.66	440.00	409.84	358.57
		490.27	450.95	452.50	451.49	450.76	384.40	391.13
		448.08	440.78	463.34	462.33	461.51	397.12	374.85
	Step cooling	361.58	386.39	/	368.66	/	383.92	338.15
		440.21	403.42		387.21		349.62	356.52
		476.71	411.49		416.07		362.99	374.23

Table A6
Cohesion and friction angle of samples after two different thermal treatments

		25 °C	200 °C	300 °C	400 °C	500 °C	600 °C	900 °C
C (MPa)	Water cooling	17.311	27.263	22.775	27.089	27.215	17.365	7.8924
		18.836	27.914	26.4963	26.476	23.375	15.802	8.4948
		20.943	28.198	1.006	27.667	31.886	18.335	9.4449
	Step cooling	19.71	18.82	/	16.23	/	13.61	11.99
		19.21	18.76		16.78		13.94	13.01
		19.06	19.12		16.98		13.29	14.27
$\phi(^\circ)$	Water cooling	67.309	63.062	66.021	62.436	62.399	64.555	67.087
		64.971	62.387	64.223	63.252	64.729	65.965	66.765
		63.766	61.908	61.957	61.594	59.474	63.675	66.520
	Step cooling	62.59	63.55	/	64.12	/	64.55	64.56
		64.804	64.31		64.52		64.92	64.54
		65.85	64.61		65.37		66.14	64.44

References

1 Kelkar S, WoldeGabriel G, Rehfeldt K. Lessons learned from the pioneering hot dry rock project at Fenton Hill, USA. *Geothermics*. 2016;63:5–14.
2 Tester JW, Anderson BJ, Batchelor AS, et al. *The Future of Geothermal Energy*. The United States: Massachusetts Institute of Technology; 2006.
3 Tran NH, Rahman SS. Development of hot dry rocks by hydraulic stimulation: natural fracture network simulation. *Theor Appl Fract Mech*. 2007;47(1):77–85.
4 Ueda A, Nakatsuka Y, Kunieda M, et al. Laboratory and field tests of CO^2–water injection into the Ogachi hot dry rock site. *Jpn. Energy Procedia*. 2009;1(1):3669–3674.
5 Heap MJ, Violay M, Wadsworth FB, Vasseur J. From rock to magma and back again: the evolution of temperature and deformation mechanism in conduit margin zones. *Earth Planet Sci Lett*. 2017;463:92–100.
6 Meredith PG, Atkinson BK. Fracture toughness and subcritical crack growth during high-temperature tensile deformation of Westerly granite and Black gabbro. *Phys Earth Planet In*. 1985;39(1):33–51.
7 Vázquez P, Shushakova V, Gómez-Heras M. Influence of mineralogy on granite decay induced by temperature increase: experimental observations and stress simulation. *Eng Geol*. 2015;189:58–67.
8 Liu S, Xu J. Mechanical properties of Qinling biotite granite after high temperature treatment. *Int J Rock Mech Min Sci*. 2014;71:188–193.
9 Géraud Y, Mazerolle F, Raynaud S. Comparison between connected and overall porosity of thermally stressed granites. *J Struct Geol*. 1992;14(8):981–990.
10 Zhang H, Guo B, Gao D, Huang H. Effects of rock properties and temperature differential in laboratory experiments on underbalanced drilling. *Int J Rock Mech Min Sci*. 2016;83:248–251.
11 Johnson B, Gangi AF, Handin J. Thermal cracking of rock subjected to slow, uniform temperature changes. *Int J Rock Mech Min Sci Geomech Abstr*. 1979;16(2):23.
12 Rocchi V, Sammonds PR, Kilburn CRJ. Fracturing of Etnean and Vesuvian rocks at high temperatures and low pressures. *J Volcanol Geoth Res*. 2004;132(2):137–157.
13 Tian H, Ziegler M, Kempka T. Physical and mechanical behavior of claystone exposed to temperatures up to 1000°C. *Int J Rock Mech Min Sci*. 2014;70:144–153.
14 Urquhart A, Bauer S. Experimental determination of single-crystal halite thermal conductivity, diffusivity and specific heat from -75 °C to 300 °C. *Int J Rock Mech Min Sci*. 2015;78:350–352.
15 González-Gómez WS, Quintana P, May-Pat A, Avilés F, May-Crespo J, Alvarado-Gil JJ. Thermal effects on the physical properties of limestones from the Yucatan Peninsula. *Int J Rock Mech Min Sci*. 2015;75:182–189.
16 Dwivedi RD, Goel RK, Prasad V, Sinha A. Thermo-mechanical properties of Indian and other granites. *Int J Rock Mech Min Sci*. 2007;45(3):303–315.
17 Hu J, Sun Q, Pan X. Variation of mechanical properties of granite after high-temperature treatment. *Arab. J. Geosci.* 2018;11(2):43.
18 Zhang W, Sun Q, Zhang Y, Xue L, Kong F. Porosity and wave velocity evolution of granite after high-temperature treatment: a review. *Environ. Earth Sci.* 2018;77(9).
19 Guo X, Zou G, Wang Y, Wang Y, Gao T. Investigation of the temperature effect on rock permeability sensitivity. *J Petrol Sci Eng*. 2017;156:616–622.
20 Liang WG, Xu SG, Zhao YS. Experimental study of temperature effects on physical and mechanical characteristics of salt rock. *Rock Mech Rock Eng*. 2006;39(5):469–482.
21 Takarli M, Prince W, Siddique R. Damage in granite under heating/cooling cycles and water freeze–thaw condition. *Int J Rock Mech Min Sci*. 2008;45(7):1164–1175.
22 Cantisani E, Pecchioni E, Fratini F, Garzonio CA, Malesani P, Molli G. Thermal stress in the Apuan marbles: relationship between microstructure and petrophysical characteristics. *Int J Rock Mech Min Sci*. 2009;46(1):128–137.
23 Masri M, Sibai M, Shao JF, Mainguy M. Experimental investigation of the effect of temperature on the mechanical behavior of Tournemire shale. *Int J Rock Mech Min Sci*. 2014;70:185–191.
24 Menaceur H, Delage P, Tang A, Conil N. The thermo-mechanical behaviour of the Callovo-Oxfordian claystone. *Int J Rock Mech Min Sci*. 2015;78:290–303.
25 Wisetsaen S, Walsri C, Fuenkajorn K. Effects of loading rate and temperature on tensile strength and deformation of rock salt. *Int J Rock Mech Min Sci*. 2015;73:10–14.
26 Favero V, Ferrari A, Laloui L. Thermo-mechanical volume change behaviour of Opalinus Clay. *Int J Rock Mech Min Sci*. 2016;90:15–25.
27 Crosby ZK, Gullett PM, Akers SA, Graham SS. Characterization of the mechanical behavior of salem limestone containing thermally-induced microcracks. *Int J Rock Mech Min Sci*. 2018;101:54–62.
28 Vagnon F, Colombero C, Colombo F, et al. Effects of thermal treatment on physical and mechanical properties of Valdieri Marble - NW Italy. *Int J Rock Mech Min Sci*. 2019;116:75–86.
29 Zhang F, Zhao J, Hu D, Skoczylas F, Shao J. Laboratory investigation on physical and mechanical properties of granite after heating and water-cooling treatment. *Rock Mech Rock Eng*. 2018;51(3):677–694.
30 Yang R, Huang Z, Shi Y, Yang Z, Huang P. Laboratory investigation on cryogenic fracturing of hot dry rock under triaxial-confining stresses. *Geothermics*. 2019;79:46–60.
31 Zhang F, Zhao J, Hu D, Shao J, Sheng Q. Evolution of bulk compressibility and permeability of granite due to thermal cracking. *Geotechnique*. 2018:1–11.
32 Shabelansky AH, Bernabe Y, Mok U, Evans JB. Temperature influence on permeability of Sioux quartzite containing mixtures of water and carbon dioxide. *Int J Rock Mech Min Sci*. 2014;70:546–551.
33 Blanco-Martín L, Rouabhi A, Billiotte J, et al. Experimental and numerical investigation into rapid cooling of rock salt related to high frequency cycling of storage caverns. *Int J Rock Mech Min Sci*. 2018;102:120–130.
34 Lehnhoff TF, Scheller JD. The influence of temperature dependent properties on thermal rock fragmentation. *Int J Rock Mech Min Sci Geomech Abstr*. 1975;12(8):255–260.
35 Griggs DT, Turner FJ, Heard HC. Deformation of rocks at 500°C to 800°C. *Geol Soc Am Mem*. 1959;257:241–270.
36 Gräf V, Jamek M, Rohatsch A, Tschegg E. Effects of thermal-heating cycle treatment on thermal expansion behavior of different building stones. *Int J Rock Mech Min Sci*. 2013;64:228–235.
37 Funatsu T, Kuruppu M, Matsui K. Effects of temperature and confining pressure on mixed-mode (I–II) and mode II fracture toughness of Kimachi sandstone. *Int J Rock Mech Min Sci*. 2014;67:1–8.
38 Shao J, Xie S, Duveau G, Masri M, Chen L. 2 - anisotropic poroplasticity in saturated porous media, effect of confining pressure, and elevated temperature. In: Shojaei AK, Shao J, eds. *Porous Rock Fracture Mechanics*. Woodhead Publishing; 2017:27–46.
39 Brotóns V, Tomás R, Ivorra S, Alarcón JC. Temperature influence on the physical and mechanical properties of a porous rock: san Julian's calcarenite. *Eng Geol*. 2013;167:117–127.
40 Shao S, Wasantha PLP, Ranjith PG, Chen BK. Effect of cooling rate on the mechanical behavior of heated Strathbogie granite with different grain sizes. *Int J Rock Mech Min Sci*. 2014;70:381–387.
41 Lion M, Skoczylas F, Ledésert B. Effects of heating on the hydraulic and poroelastic properties of bourgogne limestone. *Int J Rock Mech Min Sci*. 2005;42(4):508–520.
42 Siratovich PA, Villeneuve MC, Cole JW, Kennedy BM, Bégué F. Saturated heating and quenching of three crustal rocks and implications for thermal stimulation of permeability in geothermal reservoirs. *Int J Rock Mech Min Sci*. 2015;80:265–280.
43 Rathnaweera TD, Ranjith PG, Gu X, et al. Experimental investigation of thermomechanical behaviour of clay-rich sandstone at extreme temperatures followed by cooling treatments. *Int J Rock Mech Min Sci*. 2018;107:208–223.
44 Nara Y, Meredith PG, Yoneda T, Kaneko K. Influence of macro-fractures and micro-fractures on permeability and elastic wave velocities in basalt at elevated pressure. *Tectonophysics*. 2011;503:52–59.
45 Zhao YS, Wan ZJ, Feng ZJ, Xu ZH, Liang WG. Evolution of mechanical properties of granite at high temperature and high pressure. *Geomechanics Geophys. Geo-Energy Geo-Resour*. 2017;3:199–210.
46 Kumari WGP, Ranjith PG, Perera MSA, Chen BK. Experimental investigation of quenching effect on mechanical, microstructural and flow characteristics of reservoir rocks: thermal stimulation method for geothermal energy extraction. *J Petrol Sci Eng*. 2018;162:419–433.
47 Isaka B, Gamage R, Rathnaweera T, Perera M, Chandrasekharam D, Kumari W. An influence of thermally-induced micro-cracking under cooling treatments: mechanical characteristics of Australian granite. *Energies*. 2018;11:1338.

48 Wu Q, Weng L, Zhao Y, Guo B, Luo T. On the tensile mechanical characteristics of fine-grained granite after heating/cooling treatments with different cooling rates. *Eng Geol*. 2019;253:94–110.
49 Glover PWJ, Baud P, Darot M, et al. a/p phase transition in quartz monitored using acoustic emissions. *Geophys J Int*. 1995;120(3):775–782.
50 Zhang W, Sun Q, Hao S, Geng J, Lv C. Experimental study on the variation of physical and mechanical properties of rock after high temperature treatment. *Appl Therm Eng*. 2016;98:1297–1304.
51 Nasseri MHB, Tatone BSA, Grasselli G, Young RP. Fracture toughness and fracture roughness interrelationship in thermally treated westerly granite. *Pure Appl Geophys*. 2009;166(5-7):801–822.
52 Chaki S, Takarli M, Agbodjan WP. Influence of thermal damage on physical properties of a granite rock: porosity, permeability and ultrasonic wave evolutions. *Construct Build Mater*. 2008;22(7):1456–1461.
53 Zong Y, Han L, Wei J, Wen S. Mechanical and damage evolution properties of sandstone under triaxial compression. *Int J Min Sci Technol*. 2016;26(4):601–607.
54 Walsh JB. The effect of cracks on the compressibility of rock. *J Geophys Res*. 1965;70 (2):381–389.
55 David EC, Brantut N, Schubnel A, Zimmerman RW. Sliding crack model for nonlinearity and hysteresis in the uniaxial stress–strain curve of rock. *Int J Rock Mech Min Sci*. 2012;52:9–17.
56 Griffiths L, Heap MJ, Baud P, Schmittbuhl J. Quantification of microcrack characteristics and implications for stiffness and strength of granite. *Int J Rock Mech Min Sci*. 2017;100:138–150.
57 Zhang F, Hu DW, Xie SY, Shao JF. Influences of temperature and water content on mechanical property of argillite. *Eur J Environ Civ En*. 2014;18(2):173–189.
58 Todd TP. *Effect of Cracks on Elastic Properties of Low Porosity Rocks*. PhD thesis. Cambridge, MA: MIT; 1973.
59 Griffiths L, Lengliné O, Heap MJ, Baud P, Schmittbuhl J. Thermal cracking in westerly granite monitored using direct wave velocity, coda wave interferometry, and acoustic emissions. *J Geophys Res: Solid Earth*. 2018;123:2246–2261.
60 Zhao Y, Feng Z, Zhao Y, Wan Z. Experimental investigation on thermal cracking, permeability under HTHP and application for geothermal mining of HDR. *Energy*. 2017;132:305–314.
61 Zhang Y, Zhao G. A global review of deep geothermal energy exploration: from a view of rock mechanics and engineering. *Geomechanics Geophys. Geo-Energy Geo-Resour.* 2020;6:4.
62 Yang R, Huang Z, Shi Y, Yang Z, Huang P. Laboratory investigation on cryogenic fracturing of hot dry rock under triaxial-confining stresses. *Geothermics*. 2019;79: 46–60.
63 Wang X, Schubnel A, Fortin J, Guéguen Y, Ge H. Physical properties and brittle strength of thermally cracked granite under confinement. *J Geophys Res: Solid Earth*. 2013;118:6099–6112.
64 Zimmermann G, Reinicke A. Hydraulic stimulation of a deep sandstone reservoir to develop an Enhanced Geothermal System: laboratory and field experiments. *Geothermics*. 2010;39:70–77.
65 Ding C, Hu D, Zhou H, Lu J, Lv T. Investigations of P-Wave velocity, mechanical behavior and thermal properties of anisotropic slate. *Int J Rock Mech Min*. 2020;127: 104176.